On the Surface Deformation of a Liquid Jet Ejected from Semi-Turbulent Pipe Flow

W. Mayer, E. Laurien*, E. Khalifa* and M. Schüler**
wolfgang.mayer@dlr.de, laurien@ike.uni-stuttgart.de
German Aerospace Center, DLR Lampoldshausen, D-74239 Hardthausen, Germany
*** University of Stuttgart, IKE Department of Thermofluiddynamics, Pfaffenwaldring 31, D-70550, Stuttgart**
**** Guest Student at DLR, University of Stuttgart**

Abstract

Surface deformations of a jet ejected from a straight-pipe atomizer may be due to the turbulent fluctuations in the interior of the pipe. At relatively low Reynolds number (Re) near the transition from laminar to turbulent pipe flow (e.g. Re_l = 3000 based on the mean velocity and the pipe diameter), an unsteady semi-turbulent state exists which differs from the better known fully developed flow at higher Re. In the present work low- and high-Re jets are investigated experimentally by the DLR group. To identify the influence of the inner injector flow condition to the jet surface phenomena a special injector set-up has been designed. With this setup it was possible to eliminate relative velocity effects between jet and ambient fluid. Using shadowgraphy and a novel image processing approach, wavelengths, amplitudes and undisturbed jet length could be determined. The corresponding pipe flow is simulated numerically using Direct Numerical Simulation (DNS) by the University group. The axial mean velocity profile and turbulent intensities are smaller than those at higher Re. The computed lengths scales of the turbulent structures within the injector agree well with the observed jet surface waves. Atomization is affected when Re is reduced to the semi-turbulent state (Re_l = 3000), due to the thicker laminar envelope.

1. Introduction

Injection is affected by many different phenomena. This study takes a closer look at the effects of turbulence and on the deformation of the jet surface. Using a liquid ethanol and gaseous nitrogen combination makes it possible to see the effects on the surface of the jet from shadowgraph images [1].

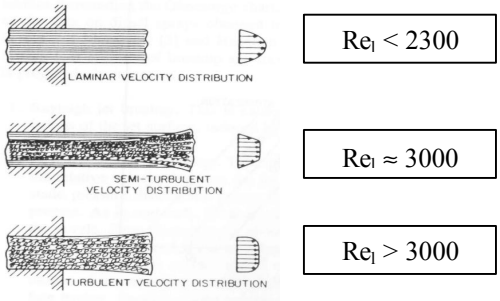

Figure 1. Various velocity distributions in jets presented in [2]

As sketched in Figure 1, the jet emerges from the nozzle in either a laminar, a semi-turbulent or fully turbulent state [2]. If the flow at the orifice is fully turbulent, the jet will disintegrate under the influence of its own turbulence. A semi-turbulent flow comprises a turbulent core and a laminar envelope. In this case, jet disintegration does not occur close to the orifice exit. However, further downstream, the faster turbulent core outpaces its protective laminar layer and then disintegrates in the normal manner of a turbulent jet.

The flow visualization picture in Figure 2 shows the jet breakup of an ethanol jet at Re_l = 3000, using a straight pipe atomizer. At this low Reynolds number the surface deformations appear only far downstream of the nozzle. This advances the concept that turbulence within the liquid jet leads to the observed instability and breakup, but has to penetrate through the laminar envelope.

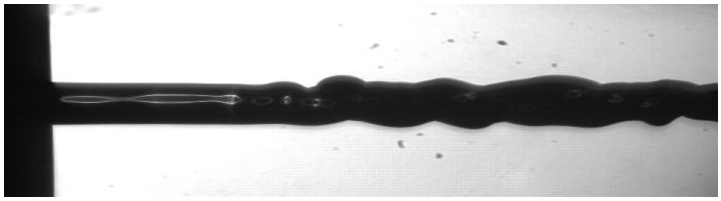

Figure 2. Visualizations of surface deformation of a free jet at Re_l = 3000 [3]

2. Experimental Setup

Figure 3 shows the pressurized chamber with the injector used in the experiments. The inner diameter of the ethanol injector is 2.2 mm, the outer diameter is 2.5 mm surrounded by the nitrogen coaxial injector with a large gap of 10 mm diameter to achieve constant relative velocities along the liquid jet. The length-to-diameter ratio of the ethanol injector tube is greater than 40 ensuring fully developed pipe flow [3]. Optical access to the chamber is provided by three windows. The figure also shows a representative shadowgraph of the flow and the characteristic wavelength (λ) and amplitude (A). The wavelength is the length of the surface structures along the axial direction (z) and the amplitude is the extension in the radial direction (r) (figure 3).

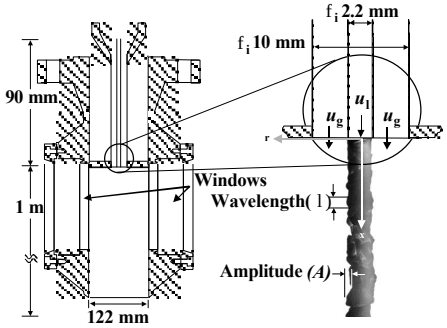

Figure 3. Test chamber, injector tip design, jet surface characteristics

u_l [m/s]	Re_l
2.2	2300
2.4	2700
2.6	3000
3.8	4300
5.0	5600
5.4	6000
9.0	10000

Table 1. injection velocities and corresponding Re number

The tests were performed at a chamber pressure of 1.0 MPa and T = 281±4K. In order to achieve a wide range of Reynolds numbers, the jet injection velocities were 2.2, 2.4, 2.6 , 3.8, 5.0, 5.4 and 9.0 m/s, corresponding to Re 2300, 2700, 3000, 4300, 5600, 6000 and 10000. The Reynolds number is calculated using the dense core flow values for this presentation.

3. Shadowgraphy

The project used a standard shadowgraph technique with a digital CCD-Camera and a xenon light. The size of the images is approximately 20 x 10 mm. The procedure digitizes the images with 256 grey levels and a resolution of 512x256 pixels corresponding to 39 μm per pixel. The targeted testing conditions were to look at jet surface phenomena, therefore, most of the testing conditions show no droplet formation. For each testing condition 4096 images were taken and used to determine the amplitude and wavelength of the surface and the undisturbed jet length. These parameters are calculated from the contour of the upper and

lower surface in each image and then averaged over all the images. The wavelength is calculated as the axial length of a surface structure on the jet and the amplitude is the radial extension of this structure (figure 3). The undisturbed jet length is determined as the smallest axial value, where a wave occurred, i.e. the initial smooth piece of the jet at the injection exit. Of course, the accuracy of the calculated wavelength and amplitude is directly dependent on the number of quality images used to determine the values, but the presented values provide reliable information showing relevant trends under these coaxial flow conditions, due to the large number of images that has been analysed.

4. Experimental Results

The results of earlier studies at DLR [3] are confirmed by this work. With a constant chamber pressure p_∞ = 1 MPa the trend for the wavelength is obvious. The magnitude of wavelength decreases with increasing injection velocity and therefore with the turbulent energy contained in the jet (figure 4 and figure 5). At the higher velocity, the turbulent kinetic energy is creating smaller surface structures and eventually droplets [3].

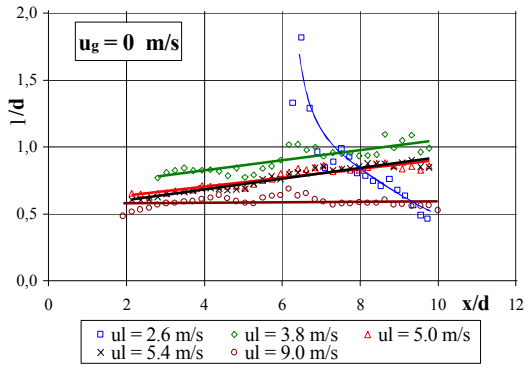

Figure 4. Wavelength (λ), p_∞ = 1 MPa

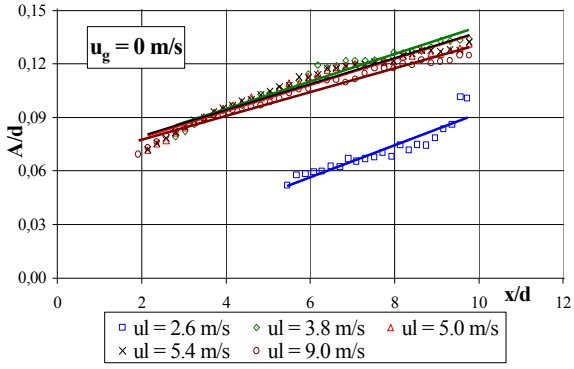

Figure 5. Amplitude (A), p_∞ = 1 MPa

In contrast, the behaviour at Re_l = 3000 is totally different. At the beginning of wave evolution we can recognize wavelengths of the dimension nearly twice the injector diameter, also the amplitude is very small (figure 4 and figure 5). Further downstream the wavelength decreases sharply to a dimension similar to the fully turbulent jets at higher Reynolds numbers with an increasing amplitude, which is still smaller than the ones at higher Reynolds numbers (figure 4 and figure 5).

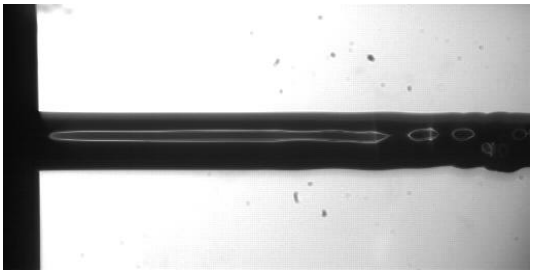

Figure 6. u_l = 2.6 m/s, u_g = 0 m/s (Re_l = 3000)

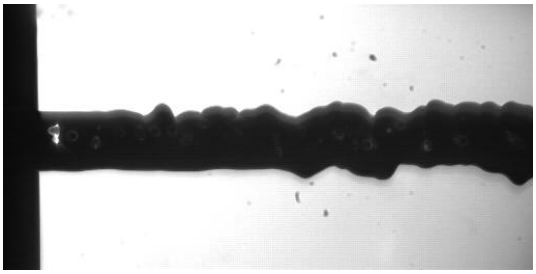

Figure 7. u_l = 3.8 m/s, u_g = 0 m/s (Re_l = 4300)

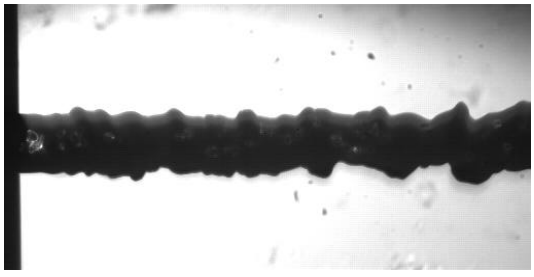

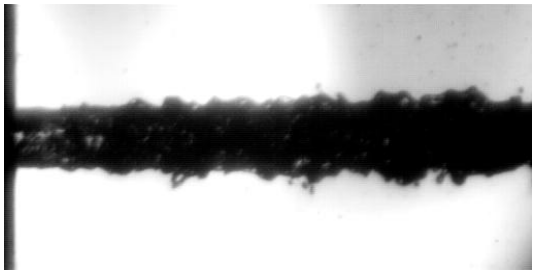

Figure 8. u_l = 5.0 m/s, u_g = 0 m/s (Re_l = 5600) **Figure 9.** u_l = 9.0 m/s, u_g = 0 m/s (Re_l = 10000)

The same trend can be seen with coaxial flow and no relative velocity. However the wavelength of a semi-turbulent jet (e.g. Re_l = 3000) is decreasing more steadily and the amplitude is nearly constant in the axial direction (figure 10 and figure 11).

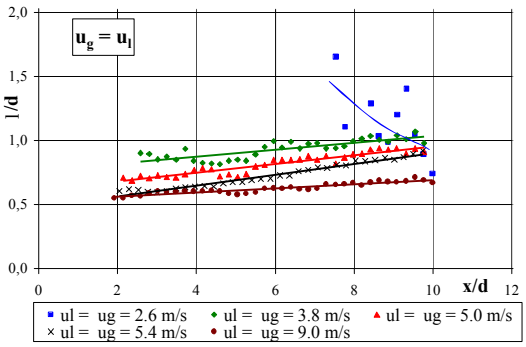

Figure 10. Wavelength (λ), p_∞ = 1 MPa

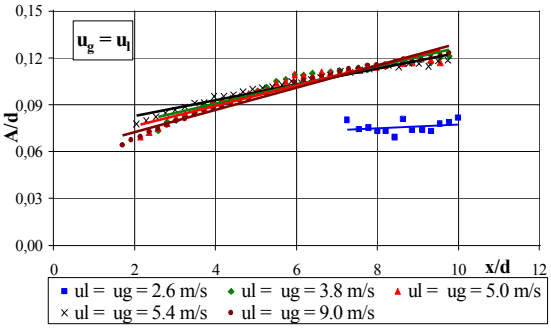

Figure 11. Amplitude (A), p_∞ = 1 MPa

These characteristics of the surface deformation of the liquid jet can be recognized by comparing the images, too (figures 6 to 9 and figures 12 to 15).

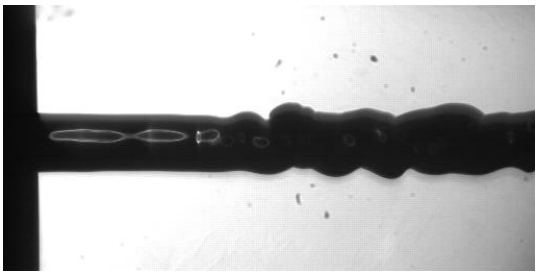

Figure 12. u_l = 2.6 m/s, u_g = 2.6 m/s (Re_l = 3000)

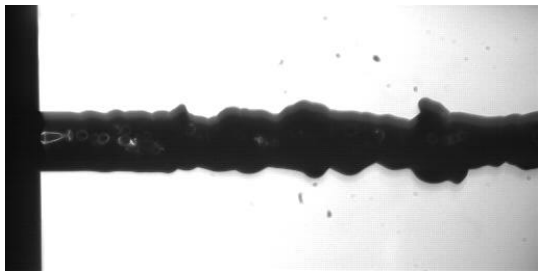

Figure 13. u_l = 3.8 m/s, u_g = 3.8 m/s (Re_l = 4300)

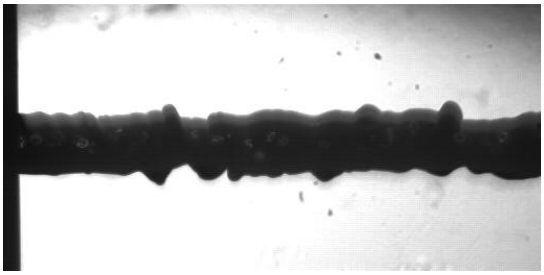

Figure 14. u_l = 5.0 m/s, u_g = 5.0 m/s (Re_l = 5600)

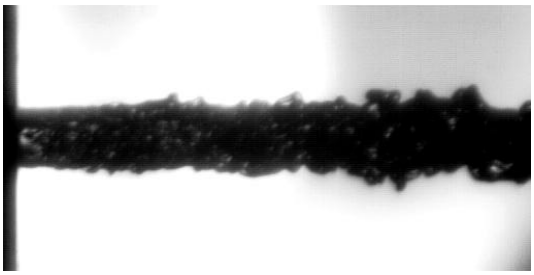

Figure 15. u_l = 9.0 m/s, u_g = 9.0 m/s (Re_l = 10000)

The undisturbed jet length does not vary significantly with injection velocity or relative velocity (e.g. Weber number) at higher Reynolds number. At lower Re the length varies considerably more. At higher relative velocity (e.g. higher Weber number) the undisturbed jet length increases. This suggests the turbulence level is much lower at low Re and has less influence on the surface disturbances, with a stabilizing effect of the aerodynamic forces. Additionally the undisturbed jet length is three to four times longer than at higher Re, due to the thicker viscous sublayer at lower Re. The range of non-dimensional values covered by the experiments is given in the appendix.

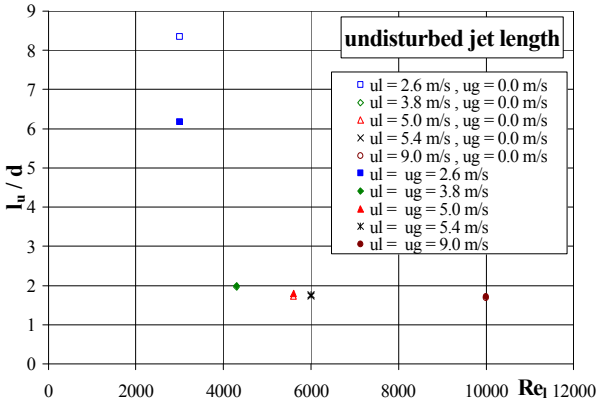

Figure 16. undisturbed jet length (l_u)

5. Numerical Simulation Method

The non-dimensional incompressible Navier-Stokes equations in cylindrical coordinates are solved using a new second order scheme [4]. The temporal differencing is also second order using Crank-Nicolson for the pressure and the linear terms and Adams-Bashforth for the non-linear terms. The scheme uses a non-staggered, structured grid. The linear equations are solved iteratively using the Preconditioned Bi-conjugate Gradient Method (PBCG) with left preconditioning. The most time consuming routines are vectorized to efficiently run on the NEC SX-5 of the High-Performance Computers Centre in Stuttgart (HLRS).

At the wall, no slip boundary conditions are imposed. To avoid the singularity at $r^* = 0$ a small "empty" core of radius $\varepsilon = 0.01$ is imposed, at which an axial "symmetry" boundary condition is imposed [4]. Periodic boundary conditions for velocity components and pressure are applied in the axial and circumferential directions. The pressure is calculated with extrapolation in the radial direction. Figure 17 shows the integration domain and the coordinate system.

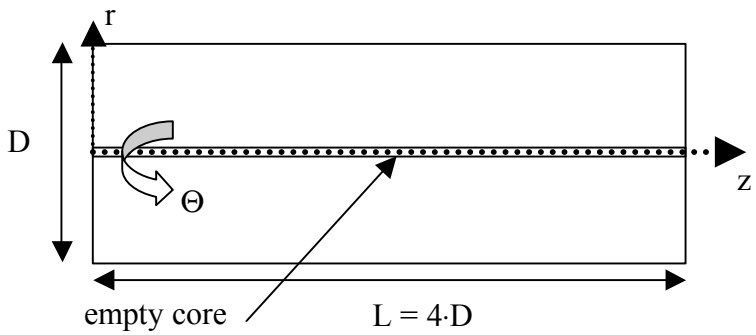

Figure 17. Integration domain and coordinate system

The numerical resolution is 40x32x99 in the circumferential, radial and axial directions, respectively. A turbulence field obtained from a high-Reynolds number simulation [5] is imposed at the beginning of the simulation. The final statistical data have been accumulated by spatial averaging in the homogeneous streamwise and circumferential directions and by time averaging over 7 data fields (one data field for every turn-over period).

6. Numerical Results

Figure 18.a shows the axial mean-velocity profile normalized by the centreline axial velocity. The numerical result is in very good agreement with detailed turbulence measurements [6] . The slope of the curve near the wall is smaller than that for higher Reynolds number (Re = 5600). Figure 18.b shows the turbulent intensities (root mean square values) of the three fluctuation velocity components normalized with the centreline velocity. The turbulent fluctuations are concentrated further away from the wall, compared with the high Reynolds number (Re = 5600). This is in accordance with the thicker viscous sublayer or envelope of the semi-turbulent case. The fluctuation intensities shown in figure 18.b are nearly of the same order of magnitude in the three directions.

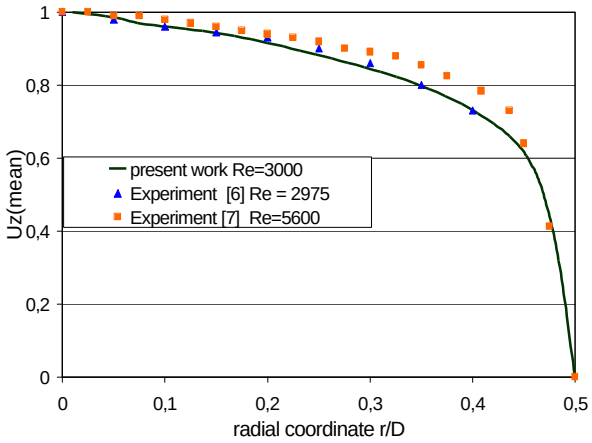

Figure 18.a

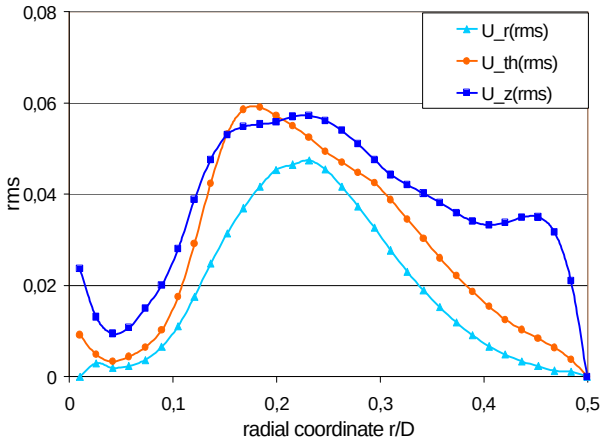

Figure 18.b

Figure 18.a : Axial mean velocity profile normalized by the centreline velocity.

Figure 18.b : Root-mean-square (rms) fluctuation velocities normalized by the centreline velocity

Figure 19.a, b, c show the isolines of the axial, radial and circumferential velocity components in an (z, r)-plane.

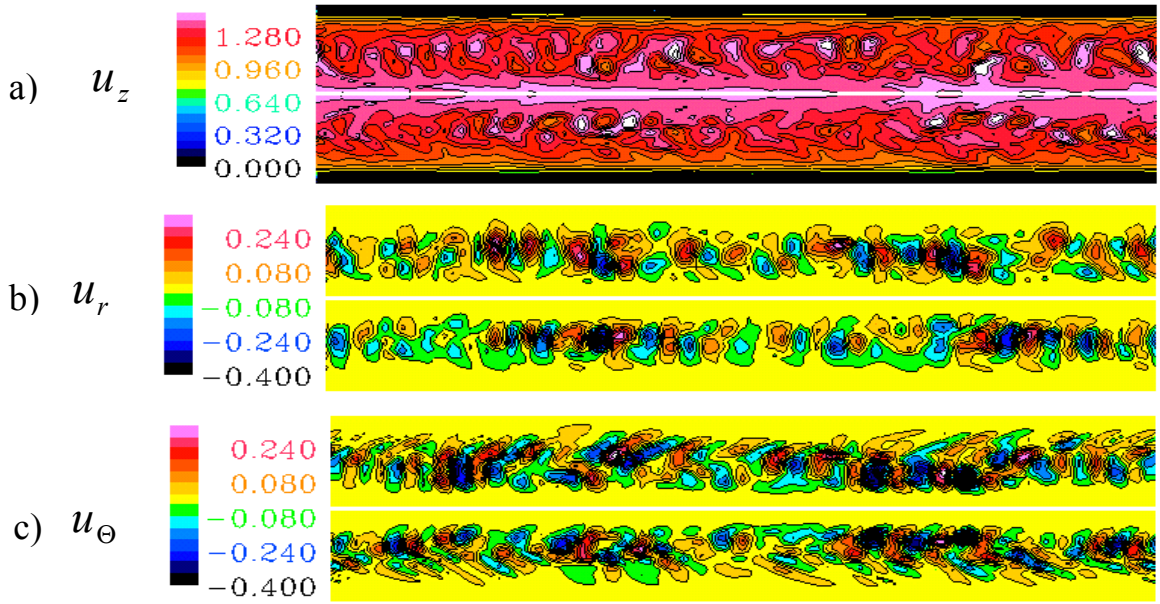

Figure 19.(a, b, c). Simulated turbulent structures of the downstream (top) , radial (middle) and circumferential (bottom) velocity components at Re = 3000.

The simulations at Re = 3000 show, that a turbulent core composed of a system of almost axisymmetric eddies exists. This turbulent core is surrounded by a laminar envelope as can be seen in figure 19.a. The laminar envelope is much thicker than the viscous sublayer existing at higher Reynolds numbers. The sweep and ejection events are clearly illustrated in figure 19.b where the positive and negative radial velocity moves to and from the wall of the atomizer. The figures 19.a, b, c are analogous to the experimentally observed "varicose" instability of low-speed jets [8]. The size of the structures is bigger than that achieved at higher Reynolds number.

Figure 20 shows the energy spectrum E(κ) showing the turbulent kinetic energy E as the y-axis and the wave number κ per unit length in a log scale as the x-axis. The energy spectrum is constant in the range $1 \le \log(k) \le 3$; i.e. $3 \le k \le 20$. The range of wavelength (λ/D) is from 2 to 0.3. This range includes the range of wavelength observed experimentally in figure 4 for $u_l = 2.6\, m/s$ ($Re_l = 3000$).

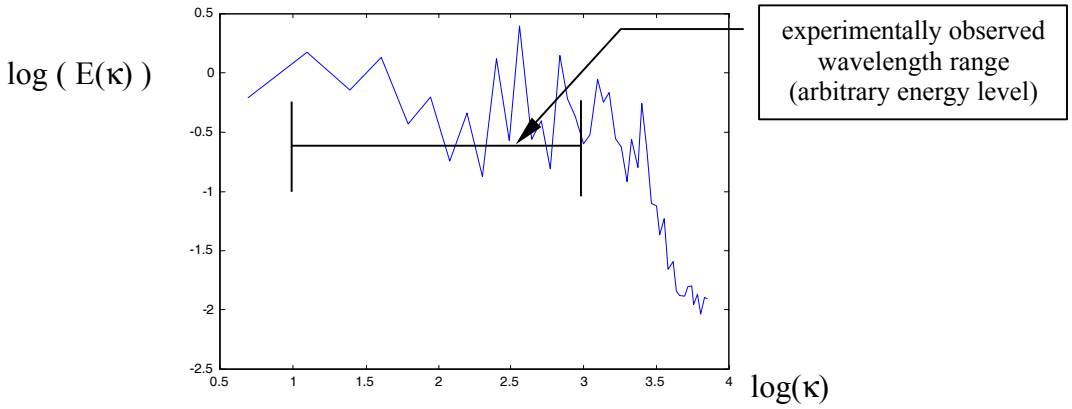

Figure 20. Energy Spectrum and experimentally observed wavelength range at $Re_l = 3000$

7. Conclusion

In coaxial jet flow conditions, the internal turbulence in the flow plays a significant part in the surface deformation. Turbulence atomization performance changes considerably, if Re is reduced from the fully turbulent to the semi-turbulent regime.
Experimentally, the undisturbed jet length for the semi-turbulent regime is larger than that at higher Reynolds numbers due to the thicker laminar envelope.
From the numerical investigation and at the semi-turbulent state ($Re_l = 3000$), varicose instability is observed and the turbulent intensities are distributed away from the wall compared with higher Reynolds number ($Re_l = 5600$). The turbulent eddies, at $Re_l = 3000$, are widely distributed with less turbulent energy.
Thus the occurrence of the surface deformations more downstream at lower Reynolds numbers compared to high Reynolds numbers can be explained as the semi-turbulent state.

Acknowledgements

We wish to recognize the efforts of G. Schneider for their contribution to this project. The present work is supported by the DFG La553/9 and the High Performance Computer Centre in Stuttgart.

Appendix

Range of non-dimensional numbers covered by the experiments :

$$Re_l = \frac{r_l \cdot d_0 \cdot u_l}{m_l} = \frac{r_l \cdot D \cdot u_m}{m_l}$$, with $d_0 = D$ and $u_l = u_m$ $\qquad 2300 < Re_l < 10000$

$$We_g = \frac{r_g \cdot d_0 \cdot (u_l - u_g)^2}{s} \qquad 0 < We_g < 110$$

$$Oh = \frac{\sqrt{We_l}}{Re_l} = \frac{m_l}{\sqrt{r_l \cdot s \cdot d_0}} \qquad 0.00671 < Oh < 0.00819$$

Nomenclature

A	amplitude
d	jet diameter
D	atomizer diameter
E	turbulent kinetic energy
l_u	undisturbed jet length
L	length
Oh	Ohnesorge number
p	pressure
r	radius
Re	Reynolds number
t	dimensionless time
u	velocity
We	Weber number
ε	radius of the empty core
ϕ	diameter
κ	wave number (presented in log. Scale)
λ	wavelength
ρ	density
μ	dynamic viscosity
Sub- and Superscripts	
*	dimensionless value
0	injection condition on the centre line, outer diameter
i	inner
l	liquid (reference value for experiments (DLR))
m	mean value (reference value for numerical simulation)
g	gas
z, r, Θ	coordinates in the axial, radial and circumferential directions
∞	properties in the chamber away from the jet flow

References

[1] Hoyt, J.W. and Taylor, J. J. "Waves on Water Jets", *J. Fluid Mech*. Vol. 83, Part 1, pp. 119-127, (1977)

[2] A. Lefebvre, "Atomization and Sprays", Hemisphere Publishing Corp., 1989

[3] R. Branam, G. Schneider, A. Volpp, W. Mayer, "Injection Characteristics on the Surface of a Coaxial Jet", JPC, AIAA Paper 2002 – 3695, Indianapolis, 2002

[4] E. Khalifa and E. Laurien, "Development of a new second and fourth order compact finite-difference scheme for the direct numerical simulation of turbulence pipe", Annual Scientific meeting GAMM 2002, March 25th – 28th 2002, Augsburg, Germany.

[5] F.O. Albina, "Private Communication", TUHH, Fluiddynamik und Schiffstheorie, 2001.

[6] V. C. Patel and M. R. Head, "Some Observations on skin friction and velocity profiles in fully developed pipe and channel flow", J. Fluid Mech. (1969), Vol. 38, part 1, pp. 181-201.

[7] J.G.M. Eggels, F. Unger, M.H. Weiss, J. Westerweel, R.J. Adrian, R. Friedlich and F.T.M. Niewstadt, "Fully developed turbulent pipe flow: a comparison between direct numerical simulation and experiment." J. Fluid. Mech. (1994), vol. 268, pp. 175-209.

[8] A. P. Johnston and K. M. Isaac, "Spray evolution of a coflowing round liquid jet in high-speed air flow", Atomization and Sprays, vol. 11, pp. 305-316, 2001.

[9] E. Khalifa and E. Laurien, "Numerical Investigation of Turbulence in the Fully Developed Regime in a Straight Pipe Atomizer", Spray 2002, Nov. 21st - 22th 2002, Freiberg, Germany